RSC Advances

PAPER

View Article Online
View Journal | View Issue

Open Access Article. Published on 27 February 2020. Downloaded on 10/16/2025 4:11:58 PM.
This article is licensed under a Creative Commons Attribution-NonCommercial 3.0 Unported Licence.

Check for updates

Cite this: *RSC Adv.*, 2020, **10**, 8580

Rotational excitation of $C_2(X^1\Sigma_g^+)$ by *para*- and *ortho*-H_2

Faouzi Najar *[ab] and Yulia Kalugina [cd]

Received 9th December 2019
Accepted 17th January 2020

DOI: 10.1039/c9ra10319h

rsc.li/rsc-advances

A new four dimensional (4D) potential energy surface for the $C_2(X^1\Sigma_g^+)$–H_2 van der Waals system is generated. The potential was obtained from a multi-reference internally contracted configuration-interaction method including the Davidson correction (MRCI+Q). The four atoms were described using the augmented correlation-consistent quadruple zeta (aug-cc-pVQZ) basis sets. Both molecules were treated as rigid rotors. Close-coupling calculations of the inelastic integral cross sections of C_2 in collisions with *para*-$H_2(j_{H_2} = 0)$ and *ortho*-$H_2(j_{H_2} = 1)$ were also carried out at low energies. After Boltzmann thermal averaging, rate coefficients were obtained for temperatures ranging from 5 to 100 K. The rate coefficients for collisions with *ortho*-H_2 are significantly larger than the rate coefficients for collisions with *para*-H_2.

1 Introduction

The C_2 molecule is one of the best known constituents of the interstellar medium. It was first detected by Souza and Lutz.[1] Subsequently, many absorption lines have been detected in the near-infrared region for the $A^1\Pi_u$–$X^1\Sigma_g^+$ Phillips system,[2–8] and in the UV region for the $D^1\Sigma_u$–$X^1\Sigma_g^+$ Mulliken system[9] and the $F^1\Pi_u$–$X^1\Sigma_g^+$ band.[10,11] The C_2 molecule is used as a diagnostic probe of the physical condition in diffuse molecular clouds. The populations of its rotational levels are determined by competition between collisional excitation and radiative excitation through absorption into excited electronic states followed by fluorescence to various vibrational levels of $X^1\Sigma_g^+$.[2] The analysis of rotationally excited C_2 provides useful information about the density of collision partners, the kinetic temperature and the strength of the radiation field permeating the gas.[12] In order to perform a more accurate analysis of C_2 excitation, rotational rate coefficients of C_2 excited by its principal interstellar collisional partner, H_2, are required. In ref. 13, the full dimensional PES was calculated by the CCSD(T)-F12a/cc-pCVTZ-F12 method. However, we suppose that there is a lack of static correlation because of the multi configurational character of the PES for interacting C_2 and H_2. In this paper, we present a new complete four dimensional (4D) PES for the ground electronic state of the C_2–H_2 collisional system calculated at the MRCI+Q level. Then, this accurate PES was used to perform rotational excitation of C_2 with both *para*-H_2 and *ortho*-H_2.

The activation energy of the $C_2 + H_2 \rightleftharpoons C_2H + H$ reaction being about 900 cm^{-1},[14] inelastic cross sections of C_2 in collisions with $H_2(j_{H_2} = 0)$ and $H_2(j_{H_2} = 1)$ are reported for total energies of up to 1000 cm^{-1} for the first 9 even rotational levels, yielding converged rate coefficients up to 100 K.

Excitation rate coefficients of C_2 excited by *para*-$H_2(j_{H_2} = 0)$ were provided by Najar *et al.*[15] In this study, the PES was derived by averaging only over three specific H_2 orientations. These calculations gave a first estimate of C_2–*para*-H_2 collisional rate coefficients. However, rotational excitation rate coefficients for C_2 in collision with *ortho*-H_2 are also needed for a complete description of C_2 excitation.[16]

The paper is organized as follows: Section 2 describes the calculation of the potential energy surface, Section 3 contains a concise description of the scattering calculations, and in Section 4, we present and discuss our results.

2 Potential energy surface

As mentioned in previous work,[17] the ground electronic state of the C_2–H_2 system is described by two dominant configurations. Because of this multi configurational character, the potential energy surface (PES) of this van der Waals complex was accomplished by first performing full valence complete active space (CASSCF) calculations[18,19] followed by multi-reference internally contracted configuration-interaction (MRCI) calculations,[20,21] including all single and double excitations from the CASSCF reference function. The contributions of higher-order excitations were estimated using the normalized multi-reference Davidson correction.[22,23] In the CASSCF-MRCI calculations, the active space is defined by distributing 10 electrons

[a]Laboratoire de Spectroscopie Atomique, Moléculaire et Application, Faculté des Sciences, Université Tunis el Manar, Tunis 2092, Tunisia. E-mail: faouzi.najar@ipeit.rnu.tn

[b]Institut Préparatoire aux Etudes d'Ingénieurs de Tunis, Université de Tunis, Tunis 1007, Tunisia

[c]Institute of Spectroscopy RAS, Fizicheskaya Str. 5, 108840 Troitsk, Moscow, Russia

[d]Department of Optics and Spectroscopy, Tomsk State University, 36 Lenin Ave., Tomsk 634050, Russia

This journal is © The Royal Society of Chemistry 2020

Open Access Article. Published on 27 February 2020. Downloaded on 10/16/2025 4:11:58 PM.
This article is licensed under a Creative Commons Attribution-NonCommercial 3.0 Unported Licence.

in 10 molecular orbitals. The $1s^2$ orbitals of the carbon atoms were kept frozen. To achieve a good description of weak interactions, the calculations were performed using a rather large aVQZ basis set of Dunning.[24–26] All *ab initio* calculations were carried out using the MOLPRO program package.[27]

The body-fixed coordinate system presented in Fig. 1 was used. The center of the coordinates is placed in the middle of the bond of the C_2 molecule. Vector **R** is directed along the *z*-axis and connects the C_2 and H_2 centers of mass. The rotation of the C_2 molecule is defined by angle θ_{C_2} and the rotation of the H_2 molecule is defined by angle θ_{H_2}, while ϕ is the dihedral angle.

The *ab initio* calculations were performed using the approximation of rigid interacting molecules with the H_2 bond length corresponding to the ground vibrational state: $r_{H-H} = 1.449$ Bohr.[28] For C_2, we used the experimental equilibrium distance $r_{C-C} = 2.348$ Bohr,[29] which differs by less than 1% from the calculated value obtained by averaging over the $\nu = 0$ wavefunction. We note that employing state-averaged geometries is a reliable approximation for including zero-point vibrational effects within a rigid-rotor PES.[30–32]

In order to determine the interaction potential $V(R,\theta_{C_2},\theta_{H_2},\phi)$, the basis set superposition error (BSSE) was corrected for all geometries with the Boys and Bernardi counterpoise scheme:[33]

$$V(R,\theta_{C_2},\theta_{H_2},\phi) = E_{C_2-H_2}(R,\theta_{C_2},\theta_{H_2},\phi) - E_{C_2}(R,\theta_{C_2},\theta_{H_2},\phi) - E_{H_2}(R,\theta_{C_2},\theta_{H_2},\phi) \quad (1)$$

where the energies of the C_2 and H_2 subsystems are computed using a full basis set of the complex. The size inconsistency was corrected for all geometries by adding the energy -33.75 cm^{-1}.

At each point R the calculations were carried out for 122 angular orientations with θ_{C_2} varying from 0° to 180°, θ_{H_2} varying from 0° to 90°, and ϕ varying from 0° to 90°. *R*-distances were varied from 4.8 to 20 Bohr, giving 29 grid points.

For the solution of the close-coupling scattering equations, it is most convenient to expand the interaction potential $V(R,\theta_{C_2},\theta_{H_2},\phi)$ into the angular functions at each value of R. For the scattering of two linear rigid rotors, we used the expansion of Green:[34]

$$V(R,\theta_{C_2},\theta_{H_2},\phi) = \sum_{l_1,l_2,l} v_{l_1,l_2,l}(R) A_{l_1,l_2,l}(\theta_{C_2},\theta_{H_2},\phi) \quad (2)$$

The basis functions $A_{l_1,l_2,l}(\theta_{C_2},\theta_{H_2},\phi)$ are products of the associated Legendre polynomials P_{lm}:

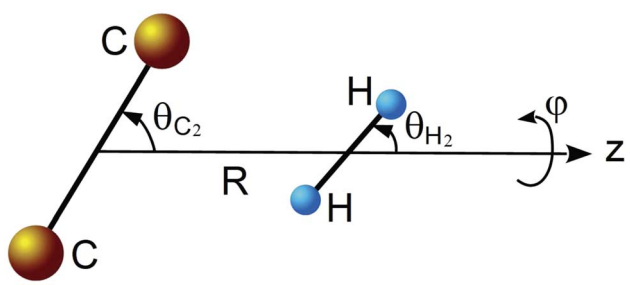

Fig. 1 Geometry describing the C_2–H_2 complex.

$$A_{l_1,l_2,l}(\theta_{C_2},\theta_{H_2},\phi) = \sqrt{\frac{2l_1+1}{4\pi}}\left\{\langle l_1 0 l_2 0 | l_1 l_2 l 0\rangle P_{l_1 0}(\theta_{C_2}) P_{l_2 0}(\theta_{H_2}) + 2\sum_m (-1)^m \langle l_1 m l_2 - m | l_1 l_2 l 0\rangle P_{l_1 m}(\theta_{C_2}) P_{l_2 m}(\theta_{H_2}) \cos(m\phi)\right\} \quad (3)$$

where $\langle \ldots | \ldots \rangle$ is a Clebsch–Gordan coefficient. The P_{lm} functions are related to coupled spherical harmonics through $Y_{lm}(\theta,\phi) = P_{lm}(\theta)e^{(im\phi)}$. Here l_1 and l_2 are associated respectively with the rotational motion of C_2 and H_2, and $l = |l_1 - l_2|, \ldots, |l_1 + l_2|$. In eqn (2), the homonuclear symmetry of the interacting molecules forces the indexes l_1 and l_2 to be even.

To obtain the expansion described above, at each point of the radial grid R we fitted the *ab initio* points to expression (2) using a linear least squares method, with $l_1^{max} = 6$ and $l_2^{max} = 4$. The choice of such expansion parameters limits the results to a total of 28 radial expansion coefficients $v_{l_1,l_2,l}(R)$. The root-mean-square error (rmse) of the fits in the long and (attractive) medium range was of the order of 10^{-3} to 10^{-2} cm^{-1}. The medium repulsive wall (energies of the order of 10^2 to 10^3 cm^{-1}) was reproduced with rmse of 1–10 cm^{-1}.

Each radial coefficient was interpolated using cubic splines for $4.8 < R \leq 16a_0$. For $R > 16a_0$ the energy (not the coefficients) was extrapolated using the $c_5/R^5 + c_6/R^6$ functional form based on its values at $R = 16a_0$ and $R = 18a_0$. For $R < 4.8a_0$ the energy was extrapolated using the functional form $A\exp(BR)$ based on its values at $R = 4.8a_0$ and $R = 5a_0$. Thus, our PES covers the whole range of R. However, we suggest to use it in the range from 3.0 to $100a_0$.

The global minimum of the 4D PES corresponds to a T-shaped structure with $\theta_{C_2} = 0°$, $\theta_{H_2} = 90°$, $\phi = 0°$ and $R = 6.92a_0$ with $V = -109.22$ cm^{-1}. In Fig. 2–4 we present the contour plots of the interaction energy surface for fixed equilibrium parameters. It is seen that there is a weak anisotropy of

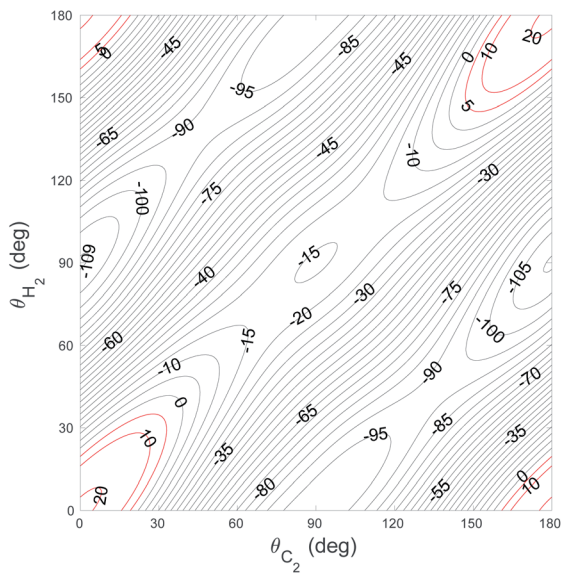

Fig. 2 Contour plot of the cut of the 4D PES for fixed $\phi = 0°$ and $R = 6.92a_0$. Energy is in cm^{-1}.

Open Access Article. Published on 27 February 2020. Downloaded on 10/16/2025 4:11:58 PM.
This article is licensed under a Creative Commons Attribution-NonCommercial 3.0 Unported Licence.

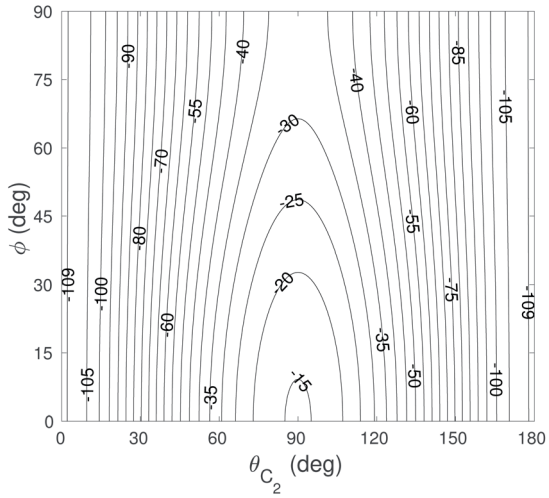

Fig. 3 Contour plot of the cut of the 4D PES for fixed $\theta_{H_2} = 90°$ and $R = 6.92a_0$. Energy is in cm^{-1}.

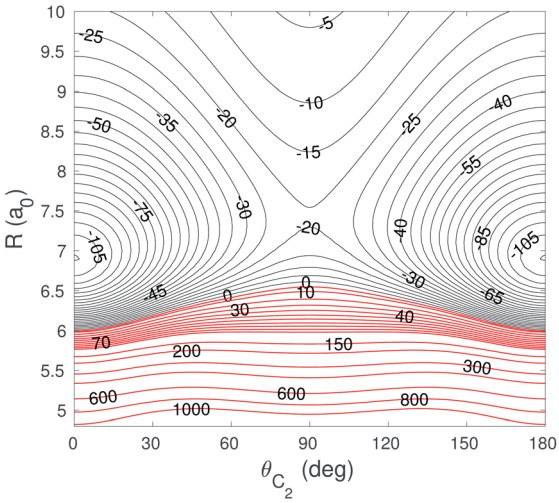

Fig. 4 Contour plot of the cut of the 4D PES for fixed $\theta_{H_2} = 90°$ and $\phi = 0°$. Energy is in cm^{-1}. Red contour lines represent repulsive interaction energies.

the PES for the Jacoby angle ϕ and a strong anisotropy for the angle θ_{C_2}. The local minimum of the PES occurs for another T-shaped structure with $\theta_{C_2} = 90°$, $\theta_{H_2} = 0°$, $\phi = 0°$ and $R = 6.70a_0$. The interaction energy at this point is $V = -101.63$ cm^{-1}.

3 Scattering study of excitation of C_2 by *para*- and *ortho*-H_2

In the present work, we consider collisions of $^{12}C_2$ with *para*- and *ortho*-H_2. Only even rotational levels j were considered here because, in homonuclear molecules with zero nuclear spins like C_2, rotational levels with odd values are not allowed. On the other hand, the H_2 molecule can exist in two forms denoted *para*- and *ortho*-H_2. In the former, the nuclear spins of the hydrogen atoms are opposed resulting in total $I = 0$, whereas, in the latter, the nuclear spins are aligned and $I = 1$. As the nuclear wavefunction must be asymmetric, in *para*-H_2, only even rotational states, $j_{H_2} = 0, 2, \ldots$ are allowed, and in *ortho*-H_2, only odd values, $j_{H_2} = 1, 3, \ldots$ are allowed.

Full close-coupling calculations[35] were carried out for total energies up to 1000 cm^{-1}, using C_2 and H_2 as rigid rotors with rotational and centrifugal distortion constants $B_{C_2} = 1.820$ cm^{-1} and $D_{C_2} = 6.92 \times 10^{-6}$ cm^{-1} (ref. 36), and $B_{H_2} = 60.853$ cm^{-1} and $D_{H_2} = 3.3 \times 10^{-6}$ cm^{-1},[29] respectively. Transitions among C_2 rotational levels up to $j = 16$ were computed for collisions involving *para*-$H_2(j_{H_2} = 0)$ and *ortho*-$H_2(j_{H_2} = 1)$. For convergence of the cross sections, the rotational states $j_{H_2} = 0$, 2 and $j_{H_2} = 1$, 3 were included in the rotational basis sets for *para*- and *ortho*-H_2, respectively. The inclusion of the $j_{H_2} = 4$ channel in *para*-H_2 affects the cross sections by less than 1 percent. For the C_2 molecule, the rotational basis set was extended up to $j_{max} = 24$ at the largest total energy considered (1000 cm^{-1}). The coupled scattering equations were solved by the MOLSCAT code[37] using the propagator of Manolopoulos.[38] For the C_2–H_2 system the reduced mass is $\mu = 1.8597$ amu. The integration parameters were chosen to ensure convergence of the cross sections in this range. The minimum and maximum integration distances chosen were $R_{min} = 3$ Bohr and $R_{max} = 50$ Bohr, respectively. The maximum value of the total angular momentum J used in the calculations was chosen according to a convergence criterion of 0.01 Å^2. The energy grid was adjusted to describe all the details of the resonances of the inelastic cross sections. The thermal rate coefficients at temperature T are obtained by averaging the rotational inelastic cross sections, $\sigma_{j\to j'}$, over a Boltzmann distribution of collision energy E_c:

$$k_{j\to j'}(T) = \left(\frac{8}{\pi\mu\beta}\right)^{1/2} \beta^2 \int_0^{\infty} E_c \sigma_{j\to j'} e^{-\beta E_c} dE_c, \quad (4)$$

with $\beta = \frac{1}{k_B T}$, where k_B is the Boltzmann constant.

4 Results

First we compare the $\sigma_{0\to 2}$ cross sections for the excitation of C_2 with *para*-$H_2(j_{H_2} = 0, 2)$ calculated with the 4D PES and including $j_{H_2} = 0$, 2 in the rotational basis set of H_2 with the cross sections for the excitation of C_2 with *para*-H_2 calculated previously by Najar *et al.*[15] with a 2D effective PES averaged over three specific H_2 orientations using equal weights of 1/3 for the three geometries considered. As we can see in Fig. 5, the two cross sections are close, having the same form of resonances with a shift and small difference in amplitudes. The difference is appreciable at high energies, approaching 35 percent. To understand where the difference comes from, we present in Table 1 cross sections at different energies for C_2-*para*H_2 calculations with a PES averaged over 3 orientations, C_2-*para*H_2 4D PES calculations with just the basis $j_{H_2} = 0$ and C_2-*para*H_2 4D PES calculations with the rotational basis involving $j_{H_2} = 0$ and $j_{H_2} = 2$ levels ($j_{H_2} = 0$, 2). We note that at low energies the major difference (~15%) is due to lack of anisotropy in the PES averaged over 3 orientations. At high energies the inaccuracies of the PES have only a minor influence on the cross sections, and

Open Access Article. Published on 27 February 2020. Downloaded on 10/16/2025 4:11:58 PM.
This article is licensed under a Creative Commons Attribution-NonCommercial 3.0 Unported Licence.

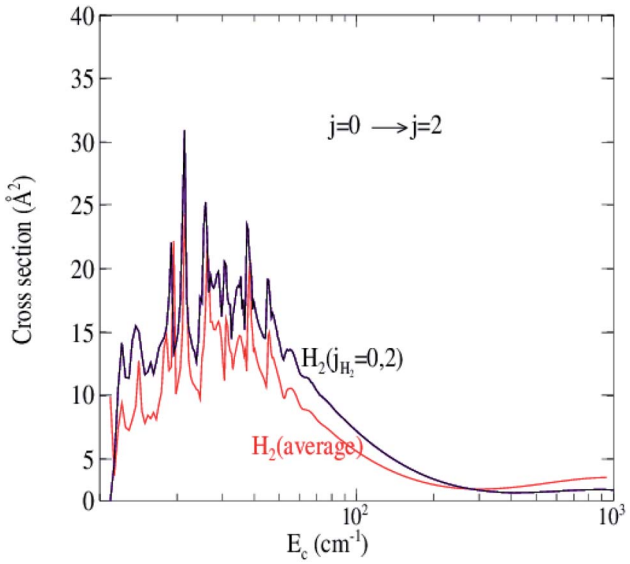

Fig. 5 Cross sections as a function of collision energy for 0 → 2 rotational excitation of C_2 with *para*-H_2 obtained by a 2D effective PES (red curve) and by the 4D PES including ($j_{H_2} = 2$) in the rotational basis set of H_2 (black curve).

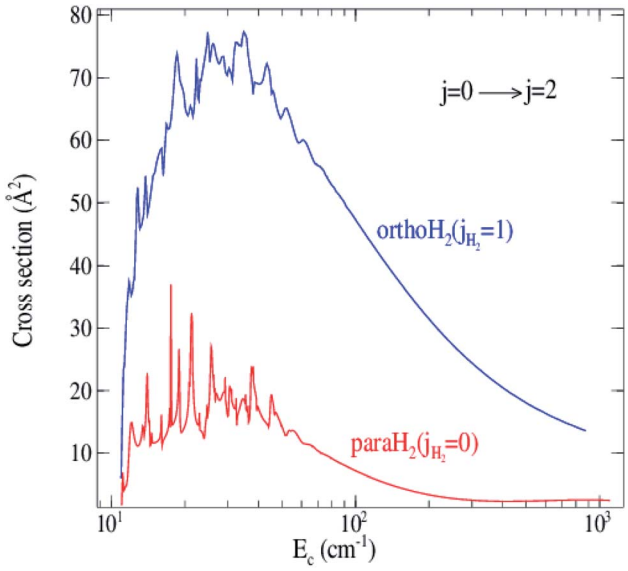

Fig. 6 Cross sections for rotational excitation of C_2 by *para*-H_2($j_{H_2} = 0$, 2) and *ortho*-H_2($j_{H_2} = 1$, 3) for the 0 → 2 transition as a function of collision energy.

Table 1 Cross sections $\sigma_{0\to2}$ (Å^2) for C_2–*para*H_2 obtained using a 2D effective PES, a 4D PES with basis $j_{H_2} = 0$ and a 4D PES with the basis $j_{H_2} = 0, 2$

Energy (cm^{-1})	2D effective PES	4D PES, $j_{H_2} = 0$	4D PES, $j_{H_2} = 0, 2$
50	11.249	13.307	14.160
100	5.613	6.580	7.087
300	2.622	2.650	2.515
500	2.978	2.819	2.379
1000	3.540	3.298	2.567

the differences stem mainly from neglect of the $j_{H_2} = 2$ rotational state. This result was also confirmed by Lique *et al.*[39] in the SiS–H_2 system.

Fig. 6 shows the collision energy dependence of the 0 → 2 inelastic integral cross sections of C_2 in collision with *para*-H_2($j_{H_2} = 0$) (including $j_{H_2} = 0, 2$) and *ortho*-H_2($j_{H_2} = 1$) (including $j_{H_2} = 1, 3$). The figure illustrates many resonances in the cross sections for collision energies below 100 cm^{-1}, which are a consequence of the temporary trapping of the H_2 molecule in the attractive potential well, involving the formation of quasi-bound states of the van der Waals C_2–H_2 complex. We note a difference in amplitude and shape of the resonances between the two cross sections. The collisions with *ortho*-H_2 are more strongly inelastic. This is expected because, unlike with *ortho*-H_2, the long-range interactions with *para*-H_2($j_{H_2} = 0$) do not involve the permanent quadrupole moment of the H_2 molecule; only induction and dispersion forces participate.[40] This behavior was also found in H_2–H_2 (ref. 41) and SO_2–H_2 (ref. 42) collisions.

Rate coefficients for rotational excitation of C_2 by *para*-H_2($j_{H_2} = 0$) and *ortho*-H_2($j_{H_2} = 1$) have been computed from cross sections generated from the grid of collision energies. The representative variation with temperature is illustrated in Fig. 7. The curves in Fig. 7 and the results in Table 2 show that the rates for *ortho*-H_2($j_{H_2} = 1$) are significantly larger by a factor of 5 on average. This result, also found previously for some systems like CO–H_2,[43] H_2O–H_2 (ref. 44) and SiS–H_2,[45] confirms the expectation that *ortho*-H_2($j_{H_2} = 1$) is a more efficient perturbant than *para*-H_2($j_{H_2} = 0$).

In the paper of Lavendy *et al.*,[46] for construction of the PES the authors considered only 5 relative orientations of C_2 and H_2

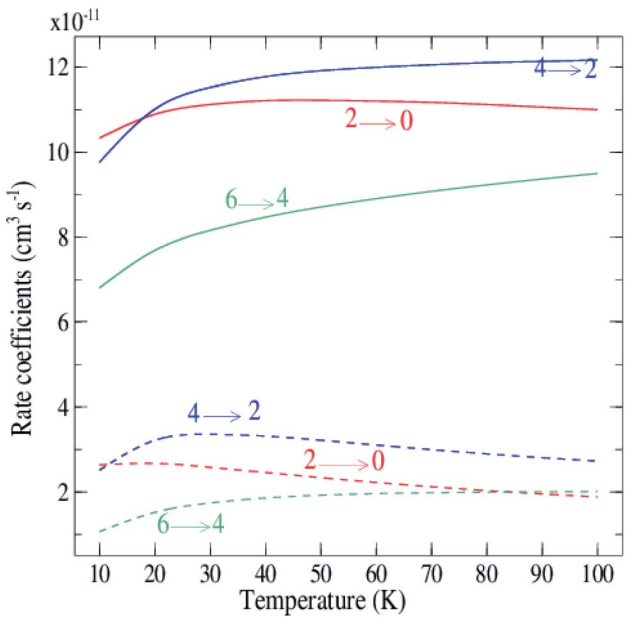

Fig. 7 Temperature dependence of rotational de-excitation rate coefficients of C_2 excited by H_2 for $\Delta j = 2$ transitions. Dashed lines: *para*-H_2($j_{H_2} = 0$); solid lines: *ortho*-H_2($j_{H_2} = 1$).

Open Access Article. Published on 27 February 2020. Downloaded on 10/16/2025 4:11:58 PM.
This article is licensed under a Creative Commons Attribution-NonCommercial 3.0 Unported Licence.

Table 2 Rate coefficients ($cm^3\ s^{-1}$) for rotational de-excitation in C_2 induced by *para*-$H_2(j_{H_2} = 0)$ and *ortho*-$H_2(j_{H_2} = 1)$. The upper entry for each transition is for $T = 50$ K, and the lower entry is for $T = 100$ K

Transition	*Para*-H_2	*Ortho*-H_2
2 → 0	0.234(-10)	1.122(-10)
	0.188(-10)	1.100(-10)
4 → 2	0.322(-10)	1.191(-10)
	0.273(-10)	1.216(-10)
6 → 4	0.192(-10)	0.870(-10)
	0.201(-10)	0.949(-10)
8 → 6	0.110(-10)	0.610(-10)
	0.141(-10)	0.704(-10)

for each R value. Later, Phillips[47] used this PES to compute the rate coefficients using the close-coupling approach. In our previous work,[15] we constructed a 2D PES based on nearly 900 *ab initio* points. For each (R,θ) we considered 3 angular orientations of the H_2 molecule, the energies of which were then averaged. In that work,[15] we compared our collision rates for C_2–*para*-$H_2(j_{H_2} = 0)$ to those of Phillips[47] for the temperature range $T < 100$ K. We found that the rates calculated by Phillips are greater by a factor of 5. This difference is due to the fact that the interaction potential used by Phillips overestimates the anisotropy of the potential. In addition, Phillips found that *para*-$H_2(j_{H_2} = 0)$ and *ortho*-$H_2(j_{H_2} = 1)$ are nearly identical colliders, which doesn't agree with our findings that there is a notable difference. This can also be explained by the fact that the potential of Phillips based on the *ab initio* energies of Lavendy *et al.* was constructed by neglecting the terms responsible for the quadrupole–quadrupole interactions.

5 Conclusions

We have applied full close-coupling calculations to investigate rotational excitation in the C_2 molecule for collisions involving *para*-$H_2(j_{H_2} = 0)$ and *ortho*-$H_2(j_{H_2} = 1)$. The calculations are performed using a highly accurate 4D potential energy surface. The inclusion of $j_{H_2} = 2$ in the rotational basis set of H_2 makes an appreciable contribution at high energies to the *para*-H_2 cross sections, approaching 35 percent. Rate coefficients for transitions among the levels of C_2 up to $j = 16$ were determined for the range of temperatures $5 \leq T \leq 100$ K. Rate coefficients with *ortho*-H_2 are larger by a factor of 5 on average than rate coefficients with *para*-H_2.

Conflicts of interest

There are no conflicts to declare.

Acknowledgements

Y. K. acknowledges financial support from the Russian Science Foundation through grant no. 17-12-01395 and grant 8.1.03.2017, and 'The Tomsk State University competitiveness improvement programme'.

Notes and references

1 S. P. Souza and B. L. Lutz, *Astrophys. J.*, 1977, **216**, L49.
2 F. H. Chaffee, B. L. Lutz, J. H. Black, P. A. Vanden Bout and R. L. Snell, *Astrophys. J.*, 1980, **236**, 474.
3 L. M. Hobbs and B. Cambell, *Astrophys. J.*, 1982, **254**, 108.
4 A. C. Danks and D. L. Lambert, *Astron. Astrophys.*, 1983, **124**, 188.
5 E. F. van Dishoeck and J. H. Black, *Astrophys. J.*, 1989, **340**, 273.
6 S. R. Federman, C. J. Strom, D. L. Lambert, *et al.*, *Astrophys. J.*, 1994, **424**, 772.
7 P. Sonnentrucker, D. E. Welty, J. A. Thorburn and D. G. York, *Astrophys. J., Suppl. Ser.*, 2007, **168**, 58.
8 M. Kaźmierczak, M. R. Schmidt, A. Bondar and J. Krelowski, *Mon. Not. R. Astron. Soc.*, 2010, **402**, 2548.
9 T. P. Snow, *Astrophys. J.*, 1978, **220**, L93.
10 D. J. Lien, *Astrophys. J.*, 1984, **287**, L95.
11 D. L. Lambert, Y. Sheffer and S. R. Federman, *Astrophys. J.*, 1995, **438**, 740.
12 E. F. van Dishoeck and J. H. Black, *Astrophys. J.*, 1982, **258**, 533.
13 H. Han, A. Li and H. Guo, *J. Chem. Phys.*, 2014, **141**, 244312.
14 N. Masakazu, M. Akira and M. Akira, *J. Phys. Chem. A*, 2009, **113**, 8963.
15 F. Najar, D. Ben Abdallah, N. Jaidane, Z. Ben Lakhdar, G. Chambaud and M. Hochlaf, *J. Chem. Phys.*, 2009, **130**, 204305.
16 R. C. Hupe, Y. Sheffer and S. R. Federman, *Astrophys. J.*, 2012, **761**(1), 38.
17 F. Najar, D. Ben Abdallah, N. Jaidane and Z. Ben Lakhdar, *Chem. Phys. Lett.*, 2008, **460**, 31.
18 P. J. Knowles and H.-J. Werner, *Chem. Phys. Lett.*, 1985, **115**, 259.
19 H.-J. Werner and P. J. Knowles, *J. Chem. Phys.*, 1985, **82**, 5053.
20 P. J. Knowles and H.-J. Werner, *Chem. Phys. Lett.*, 1988, **145**, 514.
21 H.-J. Werner and P. J. Knowles, *J. Chem. Phys.*, 1988, **89**, 5803.
22 E. R. Davidson and D. W. Silver, *Chem. Phys. Lett.*, 1977, **52**, 403.
23 S. R. Langhoff and E. R. Davidson, *Int. J. Quantum Chem.*, 1974, **8**, 61.
24 T. H. Dunning Jr, *J. Chem. Phys.*, 1989, **90**, 1007.
25 R. A. Kendall, T. H. Dunning Jr and R. J. Harrison, *J. Chem. Phys.*, 1992, **96**, 6796.
26 D. E. Woon and T. H. Dunning Jr, *J. Chem. Phys.*, 1994, **100**, 2975.
27 H.-J. Werner, P. J. Knowles, *et al.*, *MOLPRO, version 2010.1, a package of ab initio program*, 2010, http://www.molpro.net.
28 M. P. Hodges, R. J. Wheatley, G. K. Schenter and A. H. Harvey, *J. Chem. Phys.*, 2004, **120**, 710.
29 K. P. Huber and G. Herzberg, *Molecular Spectra and Molecular Structure. IV. Constants of Diatomic Molecules*, Van Nostrand Reinhold, New York, 1979.
30 P. Valiron, M. Wernli, A. Faure, L. Wiesenfeld, C. Rist, S. Kedzuch and J. Noga, *J. Chem. Phys.*, 2008, **129**, 134306.

Open Access Article. Published on 27 February 2020. Downloaded on 10/16/2025 4:11:58 PM.
This article is licensed under a Creative Commons Attribution-NonCommercial 3.0 Unported Licence.

31 Y. Scribano, A. Faure and L. Wiesenfeld, *J. Chem. Phys.*, 2010, **133**, 231105.
32 A. Faure, P. Jankowski, T. Stoecklin and K. Szalewicz, *Sci. Rep.*, 2016, **6**, 28449.
33 S. F. Boys and F. Bernardi, *Mol. Phys.*, 1970, **19**, 553.
34 S. Green, *J. Chem. Phys.*, 1975, **62**, 2271.
35 A. M. Arthurs and A. Dalgarno, *Proc. R. Soc. A.*, 1960, **256**, 540.
36 M. Martin, *J. Photochem. Photobiol., A*, 1992, **66**, 263.
37 J. M. Hutson and S. Green, *MOLSCAT Computer Code, version 14,* Distributed by Collaborative Computational Project No. 6 of the Engineering and Physical Sciences Research Council, UK, 1994.
38 D. E. Manolopoulos, *J. Chem. Phys.*, 1986, **85**, 6425.
39 F. Lique, R. Tobola, J. Klos, *et al.*, *Astron. Astrophys.*, 2008, **478**, 567.
40 D. R. Flower, J. M. Launay, E. Kochanski and J. Prissette, *Chem. Phys.*, 1979, **37**, 355.
41 G. Danby, D. R. Flower and T. S. Monteiro, *Mon. Not. R. Astron. Soc.*, 1987, **226**, 739.
42 J. Cernicharo, A. Spielfiedel, C. Balança, *et al.*, *Astron. Astrophys.*, 2011, **531**, A103.
43 A. R. Offer, M. C. van Hemert and E. F. van Dishoeck, *J. Chem. Phys.*, 1994, **100**, 362.
44 M. Wernli, P. Valiron, A. Faure, L. Wiesenfeld, P. Jankowski and K. Szalewicz, *Astron. Astrophys.*, 2006, **446**, 367.
45 J. Klos and F. Lique, *Mon. Not. R. Astron. Soc.*, 2008, **390**, 239.
46 H. Lavendy, J. M. Robbe, G. Chambaud, B. Levy and E. Roueff, *Astron. Astrophys.*, 1991, **251**, 365.
47 T. R. Phillips, *Mon. Not. R. Astron. Soc.*, 1994, **271**, 827.